J Solid State Electrochem (2009) 13:343–351
DOI 10.1007/s10008-008-0545-z

ORIGINAL PAPER

Effects of gas bubbles on the concentration profiles and conversion efficiency of three-dimensional packed-bed electrodes

Mahmoud M. Saleh

Received: 8 December 2007 / Accepted: 11 March 2008 / Published online: 10 April 2008

Abstract The effects of evolving gas bubbles on the concentration profile and conversion efficiency of three-dimensional packed-bed electrode was simulated for the first time, taking account of material balance, bubble, ohmic, kinetic, and mass transfer effects. The model produced different dimensionless groups and parameters that control the behavior of the packed-bed electrode under potentiostatic conditions. The effects of the different groups on the conversion efficiency, concentration, polarization, and current profiles were studied. Higher conversion efficiency were obtained at higher values of ω $\left(\omega = \frac{I_0 L}{nFDC_b}\right)$, lower values of δ $\left(\delta = \frac{vL}{D}\right)$ and higher values of the bubble group, ξ $(\xi = \frac{v\gamma}{I_o})$. Gas bubble formation retarded the operation at higher conversion efficiency. In presence of gas bubble, lower values of δ were required to obtain as much as conversion efficiency obtained when the gas bubble formation is absent. Also, the bubble formation retarded the operation at lower flow rates as it causes lower obtainable current and non-uniform distributions of the currents. A case study was introduced for understanding the separate important operating conditions, e.g., flow rate. Account of gas bubble effects on the concentration profiles for such system is crucial.

Keywords Gas bubbles · Packed-bed electrode · Gas bubble formation · Potentiostatic condition · Flow rate

Introduction

It is an ultimate goal of three-dimensional packed-bed electrode to obtain maximum possible conversion efficiency for the flowing reactant. The conversion efficiency, ψ, can be defined as:

$$\psi = 100x\left[1 - \frac{C_L}{C_b}\right] \quad (1)$$

where C_L and C_b are the concentrations of the reactant in the outlet and at the inlet electrolyte, respectively (see Fig. 1). Although the subject was discussed and modeled several times [1–5], it has not been modeled or discussed for gas generating porous electrode system. In ordinary flow system (non-generating gas bubbles), the conversion efficiency increases with the decrease in electrolyte flow rate. This is because the residence time increases and allows for better conversion efficiency. In gas bubble generating porous electrode, the situation is different. As the flow rate decreases, the accumulated gas bubble causes an increase in the polarization (lower currents) of the porous electrode, and it causes non-uniform distributions of the current as well [6–8]. The last is responsible for lower utilization of the porous electrode and, hence, lower effectiveness factor [9]. It was previously proposed [10, 11] to operate the gas generating porous electrodes at higher flow rates which offer lower degree of bubble accumulation inside the pores. The electrolyte flow sweeps the bubbles out of the pores causing lower overall polarization and considerable uniform current and potential distributions. However, lower conversion efficiency (practically <5%) was assumed in this case. Thus, increasing the flow rate for such systems offer lower accumulation of gas bubbles but gives lower conversion efficiencies. This situation calls for mathematical modeling to study and optimize such effects. Higher conversions system, e.g., reduction of nitrate and nitrite ions to gaseous products is important from engineering and technological point of view [12, 13]. Optimization of such system for maximum conversion efficiency can help guide the application of electrochemical systems in destruction of wastes from

M. M. Saleh (✉)
Chemistry Department, Faculty of Science, Cairo University, Cairo, Egypt
e-mail: mahmoudsaleh90@yahoo.com

radioactive and other industrial systems that produce gases as unavoidable products. Another potential application is the production of gaseous products using porous electrode. Recently, porous electrode of Pt-coated reticulated vitreous carbon was used to generate ozone and oxygen gas from flowing sulfuric acid solutions [14]. This offers an in situ production of desirable unstable gaseous products such as ozone. However, when experimental techniques fail to offer full discussion of the system behavior, mathematical modeling can guide the design and decide trends of such complicated systems before its potential applications.

It is the aim of the present general model to simulate the effects of gas bubble formation on the conversion efficiency and profiles of reactant concentration within porous electrode operating for gas generation system from flowing solutions. The model is developed and discussed under the present theory of porous electrodes taking into account the material balance, gas bubble formation, mass transfer, ohmic, and kinetics of the present system.

Development of the mathematical model

Figure 1 depicts a schematic representation of the packed-bed compartment, counter-electrode, and direction of the electrolyte flow. The position of the counter-electrode was chosen to be downstream to avoid the problems associated with the gas bubbles which are generated excessively at the polarized face of the working electrode and which were not taken into consideration in previous studies [15, 16]. The reaction considered here is the reduction of ionic species to gaseous product at the porous cathode. The following assumptions were taken into consideration during the model development. Ionic migration, axial diffusion, and dispersion effects are negligible. The packed-bed electrode has uniform porosity and assumed to be made of an inert substrate. The kinetics expression that governs the electrochemical reaction is given by Butler–Volmer equation,

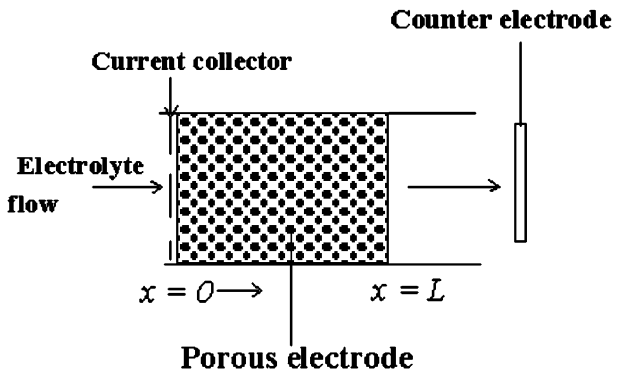

Fig. 1 Schematic representation of the packed-bed compartment and electrolyte flow

which involves a two-electron transfer rate-determining step. The reaction is first order in the active ion concentration.

Because the model accounts for considerable conversion efficiency per single pass, it is obvious to consider the material balance inside the porous bed. In presence of excess supporting electrolyte, the contribution of electrical migration of reacting species is negligible to the overall rate mass transfer, which is dominated by diffusion and convection. Plug flow of electrolyte was assumed with uniform velocity within the bed. A material balance equation is given by [17, 18]:

$$D\frac{d^2C(x)}{dx^2} - \upsilon\frac{dc(x)}{dx} = \frac{1}{nF}\frac{di_2(x)}{dx} \tag{2}$$

where dC/dx and di_2/dx are the gradient of concentration and of the solution (ionic) current inside the porous electrode, respectively.

The current in the solution phase (ionic current), i_2 is correlated to the gradient of the potential in the solution phase by:

$$i_2(x) = -\kappa(x)\frac{d\Phi_2}{dx} \tag{3}$$

where $\kappa(x)$ is the pore electrolyte conductivity and it varies with the distance inside the bed. It depends on the composition and extent of bubble generation within the pore electrolyte (see Eq. 9). The gradient of potential at the solid is related to the electronic current by ohm's law:

$$i_1(x) = -\sigma\frac{d\Phi_1}{dx} \tag{4}$$

where σ is the matrix conductivity, and it is assumed to be constant within the bed. Combining Eqs. 3 and 4 gives:

$$\frac{d\eta(x)}{dx} = \frac{i_2(x)}{\kappa(x)} - \frac{i_1(x)}{\sigma} \tag{5}$$

Because the present case is a cathodic reaction, the conductivity of the matrix is much higher than that of the solution and, hence, Eq. 5 can be reduced to;

$$\frac{d\eta(x)}{dx} = \frac{i_2(x)}{\kappa(x)} \tag{6}$$

A kinetic expression for the electrochemical reaction is given by Butler–Volmer equation [19]:

$$\frac{di_2(x)}{dx} = \frac{i_0 S\left[1 - e^{\frac{2\eta(x)}{b}}\right]}{e^{\frac{\beta\eta(x)}{b}} + \frac{i_0}{i_L(x)}} \tag{7}$$

The local limiting current $i_L(x)$ is a function of the local reactant concentration, $C(x)$ such that;

$$i_L = nF\,k_m C(x) \tag{8}$$

where k_m is the mass transfer coefficient and can be obtained from literature [20].

The pore electrolyte conductivity, $\kappa(x)$ is correlated to the electrolyte conductivity in the bulk outside the pores, κ^{o} by Bruggeman's equation; [21, 22]

$$\kappa(x) = \kappa^{0}[\theta - \varepsilon(x)]^{1.5} \tag{9}$$

where $\varepsilon(x)$ is the gas void fraction and is proportional to the ionic current, i_2, and can be given by [11]:

$$\varepsilon(x) = \frac{\theta i_2(x)}{\upsilon\lambda + i_2(x)} \tag{10}$$

i_2 represents the integration of all local reaction current that produce the gas up to point x (see [11] for derivation). Note that υ *i*s the superficial flow rate and λ is the coefficient of Faradaic gas generation which is a factor converting the solution current to volume of the generating gas bubbles, such that; [11]

$$\lambda = \frac{2PF}{RT} \tag{11}$$

Assuming ideal gas behavior and two Faradaic electrons per 1 mol of the evolved gas (as 2 appears in Eq. 11), λ equals 7.9 C cm^{-3} at standard temperature and pressure.

Equations 2, 6, 7, 9, and 10 describe the behavior of the porous electrode and give the profiles of the variables C, i_2, η, κ, and ε within the porous electrode. Substituting dimensionless variables: $\overline{C} = \frac{C}{C_b}$, $\overline{i} = i/I_0$, $\overline{\eta} = \frac{\eta}{b}$, $\overline{\kappa} = \frac{\kappa}{\kappa^0}$, and $y=x/L$, one can obtain the system of equations in dimensionless form as follows:

$$\frac{\mathrm{d}^2\overline{C}(y)}{\mathrm{d}y^2} - \delta\frac{\mathrm{d}\overline{C}(y)}{\mathrm{d}y} = \omega\frac{\mathrm{d}\overline{i}_2(y)}{\mathrm{d}y} \tag{12}$$

$$\frac{d\,\overline{\eta}(y)}{d\,y} = [\Lambda\overline{\kappa}(y)]^{-1}\overline{i}_2(y) \tag{13}$$

$$\overline{\kappa}(y) = [\theta - \varepsilon(y)]^{1.5} \tag{14}$$

$$\varepsilon(y) = \frac{\theta\overline{i}(x)}{\xi + \overline{i}(x)} \tag{15}$$

$$\frac{\mathrm{d}\overline{i}_2(y)}{\mathrm{d}y} = \frac{\left[1 - e^{2\overline{\eta}(y)}\right]}{e^{\beta\overline{\eta}(y)} + \frac{I}{\overline{C}(y)}} \tag{16}$$

The above system of five equations represents a dimensionless model and has led to some dimensional and dimensionless groups and parameters which are listed in Table 1. The boundary conditions for the above system are:

1. @ y=0

$$\overline{C} = 1, \overline{i} = 0, \frac{\mathrm{d}\overline{\eta}}{\mathrm{d}y} = 0, \varepsilon = 0, \overline{\kappa} = \theta^{1.5} \tag{17}$$

2. @ y=1

$$\frac{\mathrm{d}\overline{C}}{\mathrm{d}y} = 0, \overline{\eta} = \eta_L \tag{18}$$

where η_L is the dimensionless polarization at the exit face i.e., at γ=1(x=L).

The above system of equations (Eqs. 12–16) along with boundary conditions Eqs. 17 and 18 were solved with a numerical technique developed by Newman [23]. For seeking simplicity, the bars over the dimensionless variables are going to be dropped in the coming discussion.

Results and discussion

Results of the dimensionless model

The model calculations were performed under potentiostatic conditions. The effects of different controlling groups on the conversion efficiency and profiles of different variables (C, η, and i_2) will be explored. Because the effects of the groups I_o and I were discussed in previous works, they will be kept constant throughout the present work. The used values of I_o and I are 0.025 and 5×10^{-4}, respectively. Figure 2 shows the effects of the δ group on the concentration profile with the packed-bed at η_L=−6.0 and ω=2.5. As δ decreases the concentration at the outlet of the bed, C_L goes to lower values indicating higher conversion efficiency. The δ group included important hydrodynamic and structural parameters. Lower values of δ mean lower flow rates, υ, or higher diffusion coefficient, D at fixed value of the thickness L (because ω has a fixed value). At extremely low value of δ (δ<20), the concentration approaches zero at a bed depth of about half indicating

Table 1 Dimensional and dimensionless parameters and groups

Group	Definition
δ	$\delta = \frac{\upsilon L}{D}$
ω	$\omega = \frac{I_0 L}{nFDC_b}$
I	$I = \frac{i_0}{nFK_m C_b}$
$\xi = \frac{\upsilon\lambda}{I_0}$	Dimensionless bubble group
I_o=i_oSL	Total exchange current density
Λ=κ^ob/$I_o L$	Dimensionless conductivity group
β=0.5	Charge transfer coefficient
θ=0.7	Porosity

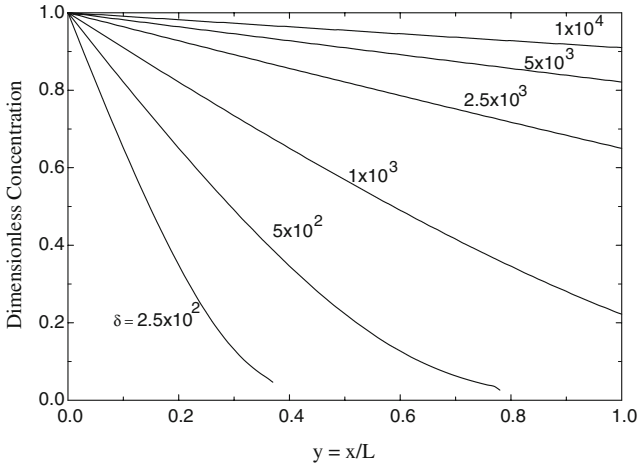

Fig. 2 Concentration profiles at different values of the group δ at η_L=−6.0 and at ω=2.5. No ohmic or gas bubble effects included

high degree of conversion. On the other hand, at higher value of δ (δ>10^4), the dimensionless concentration approaches unity, which means conversion efficie1ncy of ~0 (see Eq. 1).

Figure 3 shows the effects of the ω group on the concentration profile at δ equals 10^3 and η_L=−6.0. As ω increases, the concentration decreases significantly to lower values. A dramatic effect is shown at ω=10, where the concentration approaches zero at about half of the bed. As ω increases the total exchange current density, I_o, bed thickness, L, increases and/or bulk concentration C_b decreases (because D has a fixed value by fixing the value of δ; see Table 1). The conductivity group and the bubble groups have high values and yet, the contribution of ohmic effects is neglected. Uniform polarization profile is obtained in such case (see Eq. 13). This helps to investigate the effects of δ and ω separately without any contribution of the ohmic effects. It can be concluded from Figs. 2 and 3 that hydrodynamic and structural effects are important and predominant in determining the conversion efficiency and the concentration profile although the polarization $\eta(y)$ is uniform everywhere within the bed. Conversion efficiency increases with the increase in the increase in the residence time, i.e., the increase in the thickness and/or decrease in the flow rate. This is in agreement with the trends shown here in Figs. 2 and 3. The above effects of δ and ω are similar to what is reported in literatures in absence of gas bubbles [17, 18].

Figure 4 shows the effects of the conductivity group, Λ on the concentration profile within the bed at δ=5×10^2 and ω=2.5 at the conditions of no bubble formation. This can help to explain separate effects of ohmic drop within the bed. The concentration profile goes to lower values as Λ increases. The current profile is more uniformed at higher values of Λ and, yet, higher total current are obtained (see Eq. 6). As Λ decreases, the polarization, $\eta(y)$, becomes more non-uniformed, and higher values of η are obtained at the front than that at the back of the electrode (see Eq. 6 and Fig. 6). At y→1 (front face of the electrode), the concentration of the reactant has higher values because it was not consumed early at the back of the electrode (because η has lower values), and yet, higher concentrations support higher driving force (higher currents) at the front and, consequently, the concentration dropped to lower values at y→1 as seen in the concentration profile shown in Fig. 4. Butler–Volmer equation implies that the polarization, η, and the concentration, C, are important driving forces for higher currents. At higher values of Λ (Λ>5×10^2), the polarization is uniform everywhere and can support higher currents early at the back of the electrode;

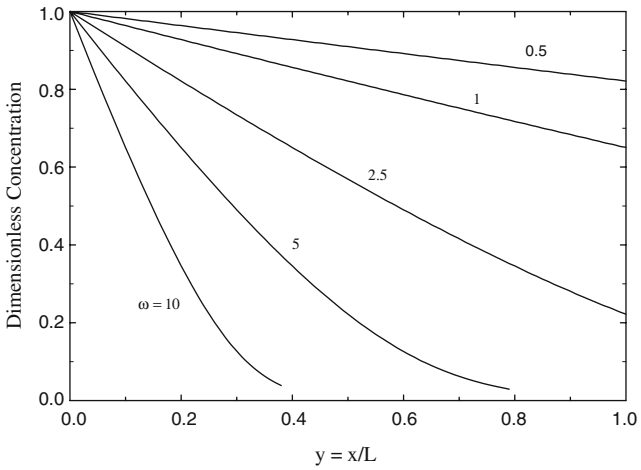

Fig. 3 Concentration profiles at different values of the group ω at η_L=−6.0 and at δ=1×10^3. No ohmic or gas bubble effects included

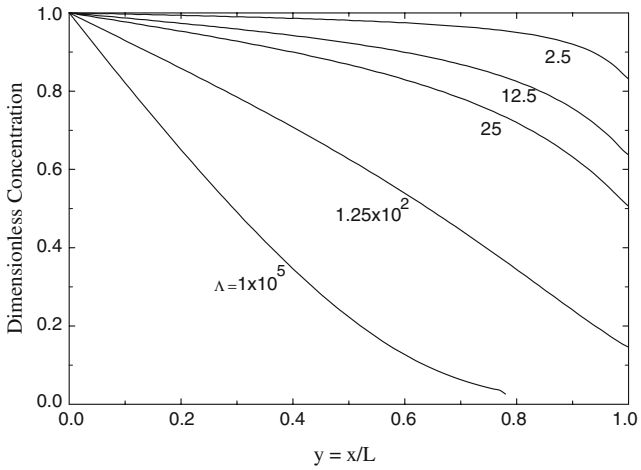

Fig. 4 Effects of the conductivity group, Λ, on the concentration profiles at η_L=−6.0 and at δ=5×10^2 and ω=2.5. No gas bubble effects included

hence, the reactant may be consumed, and lower concentrations can be obtained at one half or three fourths of the bed thickness.

The unavoidable gas bubble formation, and its influence on such gas generating systems, is crucial. The generated gas bubbles decrease the cross-sectional area available for the ionic flow and, consequently, decrease the effective conductivity of the pore electrolyte (see Eqs. 14, 15). We report here the effects of the bubble formation on the concentration profiles and the conversion efficiency. The bubble group, ξ (see Eq. 15), is a measure of the bubble formation extent. Lower values of ξ mean lower electrolyte flow rates and/or higher total exchange value, I_o. This implies higher extent of bubble formation and the reverse is true for higher values of ξ.

Figure 5 shows the effects of the bubble group, ξ, on the concentration profile at $\delta=5\times10^2$ and $\omega=2.5$ and $\Lambda=5\times10^2$. As ξ increases, the concentration profiles shifted to lower values and the reactant concentration exit at C_L of values depend on ξ. Higher values of ξ means higher flow rates. Higher flow rates help the bubbles out of the pores, resulting in lower polarization within the bed and, hence, higher currents. This adverse effect of υ is due to fixing the value of δ. This point can be clarified if the dimensional model is solved and, hence, υ will affect both υ and ξ. The results will be an overall effect of υ on the process (see "Case study"). The effects of ξ on the concentration profile can be further discussed by studying the polarization profile (Fig. 6) and current profile (Fig. 7).

In Fig. 6, as ξ increases the polarization, $\eta(y)$ becomes more uniformed within the porous electrode. As ξ increases, lower degrees of gas accumulation were obtained; hence, $\eta(y)$ is more uniformed in accordance with Eqs. 13 and 15. As ξ decreases, $\eta(y)$ becomes more non-uniformed and lower values of $\eta(y)$ were obtained at the back and middle of the electrode. Consequently at the back, lower driving forces (lower currents) are obtained. The above polarization profiles in Fig. 6 are reflected as current profiles in Fig. 7. The dimensionless reaction current (per unit volume), $J(y)=\mathrm{d}i_2(y)/\mathrm{d}y$ is shown in the figure. Not only do lower values of ξ cause non-uniform profiles of the reaction current but they also produce lower values of the total current. The total current is the integration of the reaction current, $J(y)$, i.e., $\int_0^1 J(y)\,dy = i_2\big|_{y=1} = \frac{i_{\mathrm{cell}}}{I_0}$. So the areas under curves in Fig. 7 give the total current. For instance, $i_2\big|_{y=1} = 171, 108, 64, 34.$ and 1 at $\xi=1\times10^6$, 50, 10, 2, and 0.3, respectively. Another feature in Fig. 7 is the drop in $J(y)$ at $y\rightarrow1$ at value of $\xi=1\times10^6$. This can be interpreted by inspection of the concentration and polarization profiles in Figs. 5 and 6. At $\xi=1\times10^6$, the polarization profile is uniform and, hence, support higher values of η everywhere within the bed (i.e., higher driving forces), even at the back of the electrode. This allows for consumption of the reactant early at the back and middle of

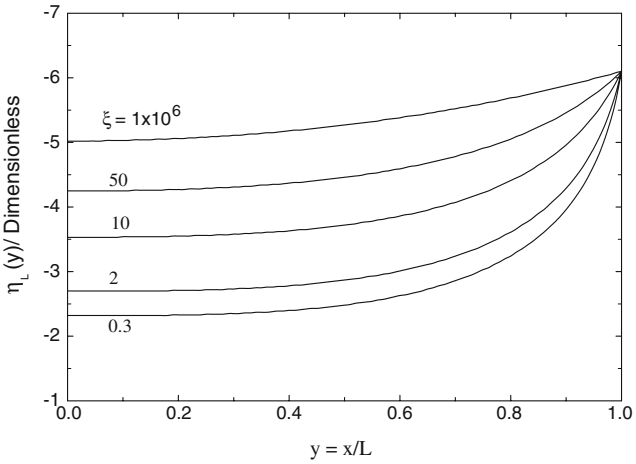

Fig. 6 Profiles of the dimensionless polarization at different values of the Bubble group ξ using the same parameters in Fig. 5

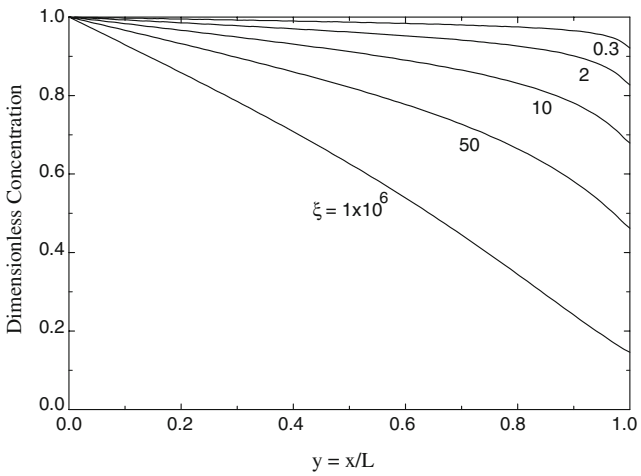

Fig. 5 Effects of the bubble group, ξ, on the concentration profiles at $\eta_L=-6.0$, $\Lambda=5\times10^2$ and at $\delta=5\times10^2$ and $\omega=2.5$

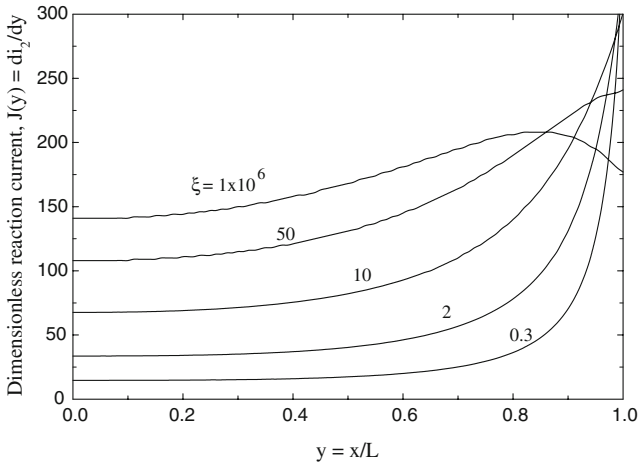

Fig. 7 Profiles of the dimensionless reaction currents at different values of the Bubble group ξ using the same parameters in Fig. 5

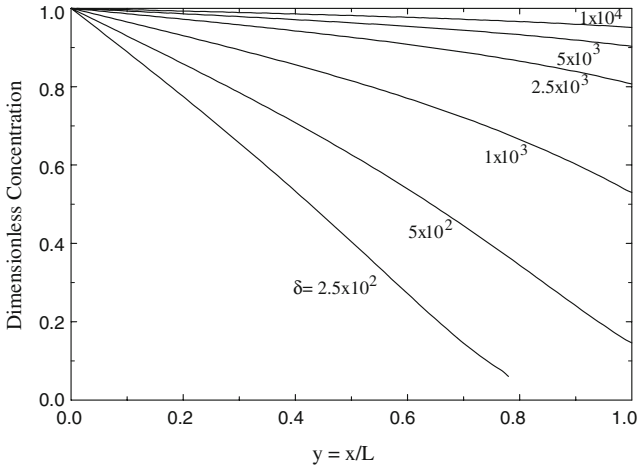

Fig. 8 Profiles of the dimensionless concentration at different values of the group δ at $\xi=1\times10^6$, $\Lambda=5\times10^2$, $\delta=5\times10^2$ and $\omega=2.5$

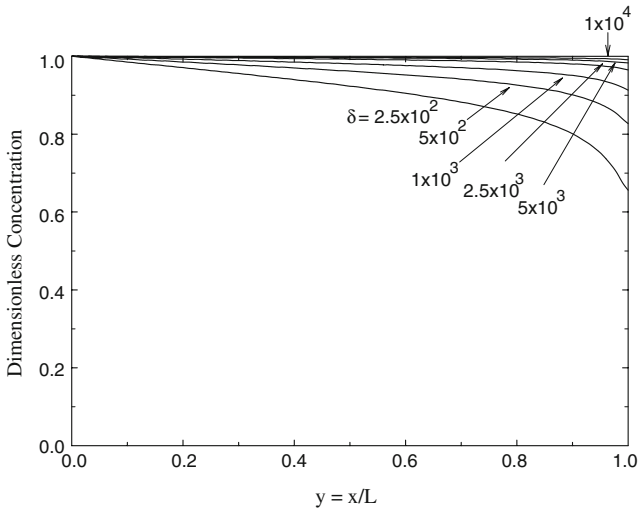

Fig. 10 Profiles of the dimensionless concentration at different values of the group δ at the same parameters of Fig. 8 but at $\xi=2$

the porous cathode, and yet, at y→1, the reactant concentration reaches lower values, and consequently, the driving force for electrochemical reaction decreases and, thus, J drops to lower values at y→1.

Figures 8, 9, and 10 show the effects of the group δ on the concentration profiles at different degrees of bubble formation. Thus, $\xi=1\times10^6$, 50, and 2 in Figs. 8, 9, and 10, respectively. As ξ decreases, the concentration profile shifts to higher values; yet, the outlet concentration have higher values indicating lower conversion efficiencies. No conversion was observed at $\xi=2$ at the highest δ values (as shown in Fig. 10). This points to the deleterious effects of gas bubble formation. One can summarize the effects of ξ on ψ by using Eq. 1 and the data in Figs. 8, 9, and 10 to account for C_L. In this case $\Psi = 100x\left(1-\overline{C}\right)$. Figure 11 shows how ψ changes with δ at the same parameters used in Figs. 8, 9, and 10. As δ increases, the conversion efficiency decreases and reaches to lower steady values at $\delta>40$. Recall that as δ increases, υ increase and/or D decreases at fixed L. As ξ decreases, the conversion efficiency decreases. The effect of ξ on ψ is more pronounced at lower δ than at higher δ values. As depicted in Fig. 11, to obtain higher values of ψ at lower values of ξ, one should use much lower values of δ, which may not be practically feasible. It is concluded that the gas bubble formation retards the operation at higher conversion efficiencies.

Case study

The previous section has shown the effects of different groups independently from each others. However, in practice, the variables are interlinked in such a way that one operating parameter can affect more than one group. It is of practical purpose to solve the dimensional model

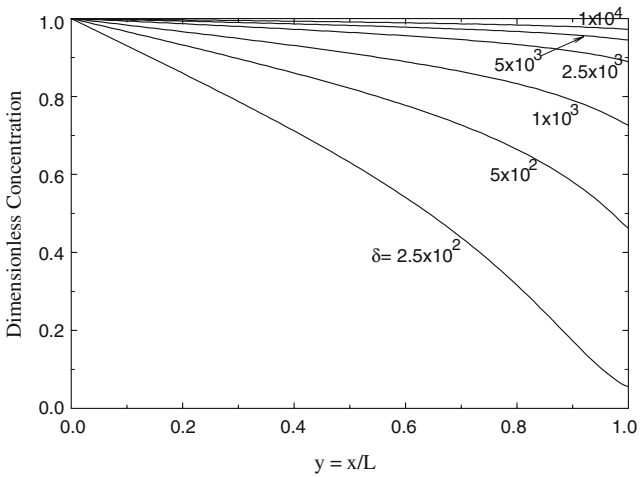

Fig. 9 Profiles of the dimensionless concentration at different values of the group δ at the same parameters of Fig. 8 but at $\xi=50$

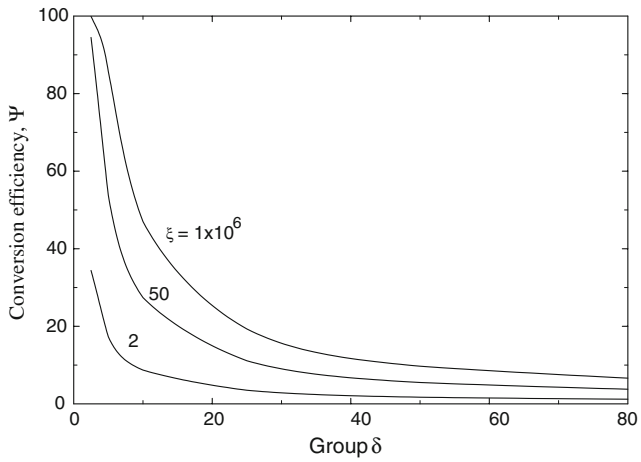

Fig. 11 Effects of the group δ on the conversion efficiency at different values of the bubble group, ξ, using the same parameters in Figs. 8, 9, and 10

Table 2 Parameters used in calculations and generation of Fig. 12 (case study)

Parameters
β=1
η_L=0.15 V
i_o=1×10^{-4} A cm^{-2}
d=0.05 cm
D=1×10^{-5} cm^2 s^{-1}
C_b=1×10^{-5} mol cm^{-3}
κ^o=0.4 ohm^{-1} cm^{-1}
L=5 cm
S=40 cm^2 cm^{-3}
θ=0.7
ν=0.01 cm^2 s^{-1}

(Eqs. 2, 5, 6–10) and study the effects of separate operating parameter. This can be done with the present case in which some real numbers are used in the calculations. One important operating parameter is the electrolyte flow rate, υ. For instance, υ affects both the bubble group, ξ, and the group δ (see Table 1). As υ increases, ξ increases, causing high conversion efficiency; meanwhile, as υ increases, δ increases, causing lower values of the conversion efficiency. It is of obvious interest to study how the flow rate, υ, affect both ξ and δ simultaneously. This will be done throughout this case study. In order to achieve such calculations, the mass transfer coefficient in Eq. 8 should be defined by using one of the available empirical correlations. In this work, an empirical formula was taken from Cussler which is given by [20]:

$$k_m = 1.17x\upsilon^{0.58}(d/\nu)^{-0.42}(\nu/D)^{-0.67} \quad (19)$$

where the symbols are defined in the Notation section. Table 2 lists the values of the parameters that were used in the calculations of this case study.

Figure 12 shows the effects of the electrolyte flow rate, υ, on the concentration profile using the parameters given in Table 2. The figure shows two cases; one when the gas bubble formation is not included in the model and the other case when the gas bubble formation is not included in the calculations. The first case can be done by putting ξ as an infinite value in Eq. 15. As υ increases, the concentration profiles shift to higher values, indicating lower conversion efficiency. It is obvious in the figure that there are considerable difference between the case when the bubble formation is included and where it is not. The difference increases as the flow rate decreases. At lower flow rates, the

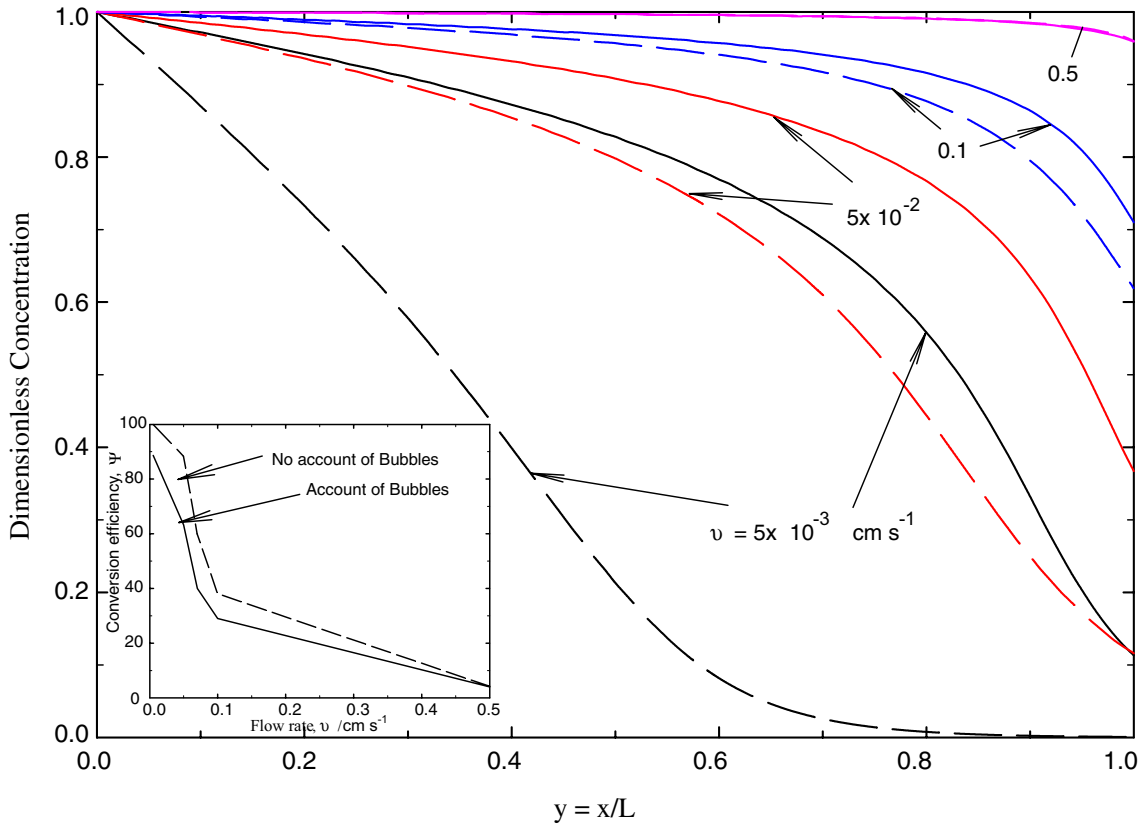

Fig. 12 Effects of the electrolyte flow rate, υ on the conversion efficiency. The figure was produced using the parameters shown in Table 2. *Solid lines* show the case where the bubble effect is included and the *dashed lines* where the bubble effect is not included

excessive gas bubbles accumulate within the bed, causing larger values of ohmic drop inside the bed and, hence, the current decease. This results in a decrease in the reaction current and led to lower conversion. The inset of Fig. 12 shows the effects of υ on ψ at the two cases of accounting and non-accounting of gas bubbles. At $\upsilon \geq 0.5$, the difference between the two cases are vanished, indicating negligible gas bubble formation. The effects of the flow rate in Fig. 12 are the combination of its impacts on the bubble group and the δ group. The results show that the bubble effects should be included in the simulation in order to obtain realistic results. This may help in better design and optimization of the operating conditions. Another effect of the gas bubbles is the enhancement of the local mass transfer due to local agitation of solution by the generating gas bubble. This will be discussed in separate article as it is out of the scope of the present work.

Summary and conclusions

A mathematical model was developed and solved numerically to account for the effects of gas bubble formation on the concentration profile and conversion efficiency of a porous cathode operating for gas generation reaction from flowing solutions. Different effects of material balance, mass transfer, ohmic, and kinetics were included in the model calculations. The gas bubble formation resulted in shifts of the concentration profiles to higher values and, hence, lower conversion efficiencies. Gas bubble effects retarded the operation of the porous electrode at higher conversion efficiency and also retarded the operation at higher values of hydrodynamic parameters which is included in the δ group. The present result may aid in better design and optimization of the operating conditions of the porous cathode. A case study was introduced, and the dimensional model was solved as well. The flow rate has dual effects on both ξ and δ. The case study showed that it is important to account for the gas bubble formation for such systems.

List of symbols

b	RT/F, V
C	concentration, mol cm^{-3}
C_b	bulk concentration, mol cm^{-3}
$\overline{C}$	dimensionless concentration
d	particle diameter, cm
D	diffusion coefficient, cm^2 s^{-1}
F	Faraday's constant, 96,500 °C mol^{-1}
i_{cell}	cell current per unit cross-sectional area of the packed-bed, A cm^{-2}
i_1	superficial local matrix current density (based on geometric area), A cm^{-2}
i_2	superficial local solution (ionic) current density (based on geometric area), A cm^{-2}
I_o	total exchange current density, i_o SL.
i_o	exchange current density based on the reaction area, A cm^{-2}
J	local reaction current per unit volume of the packed-bed, A cm^{-3}
k_m	mass transfer coefficient, cm s^{-1}
L	electrode thickness, cm
n	number of electrons transferred in the electrochemical reaction
P	pressure, atm
υ	electrolyte flow velocity, cm s^{-1}
R	gas constant, 82.06 (cm^3 atm)/(mol/K)
S	specific surface area, cm^2 cm^{-3}
T	absolute temperature, K
y	dimensionless distance within the electrode, x/L

Greek Symbols

β	charge-transfer coefficient of the electrochemical reaction
δ	dimensionless group, $\delta = \frac{\upsilon L}{D}$
λ	constant, $2PF/RT$, C cm^{-3}
ε	gas void fraction of the pore volume, dimensionless, Eq. 8
κ^o	electrolyte conductivity in the bulk outside the pores, Ω^{-1} cm^{-1}
$\kappa(x)$	pore electrolyte conductivity, Ω^{-1} cm^{-1}
ν	kinematics viscosity, cm^2 s^{-1}
Φ_1	potential in the matrix phase, V
Φ_2	potential in the solution, V
ξ	dimensionless bubble group
Λ	dimensionless conductivity group
η	polarization
θ	porosity
ψ	conversion efficiency
ω	dimensionless group, $\omega = \frac{I_0 L}{nFDC_b}$

References

1. Pilonea D, Kelsal GHL (2006) J Electrochem Soc 153:D85
2. Trainham JA, Newman J (1977) J Electrochem Soc 124:1528
3. Cheng CY, Kelsall GH, Pilone D (2005) J Appl Electrochem 35:1191
4. Ateya BG (1977) J Electroanal Chem 76:183
5. Naval JL, Oropeza M T, Ponce de León C, González-García J, Frías-Ferrer A J (2007) Hydrometal, in press

6. Ateya GB, El-Anadouli B (1991) J Electrochem Soc 138:1331
7. Saleh MM (1999) Electrochim Acta 45:959
8. Jha K, Weidner JW (1999) J Appl Electrochem 29:130
9. Saleh MM (2004) J Phys. Chem B 108:13419
10. Saleh MM, Weidner JW, Ateya BG (1995) J Electrochem Soc 142:4122
11. Saleh MM (2007) J Solid-Satate Electrochem 11:811
12. Szpyrkowicz L, Daniele S, Radaelli M, Specchia S (2006) Appl Cat B: Environmental 66:40
13. Tada K, Kawaguchi T, Shimazu K (2004) J Electroanal Chem 572:93
14. Awad MI, Saleh MM, Ohsaka T (2006) J Electrochem Soc 153: D207
15. Ateya BG, Austin L (1977) J Electrochem Soc 124:1540
16. Maltoz M, Newman J (1986) J Elecrochem Soc 133:1850
17. Alkire R, Gracon B (1975) J Electrochem Soc 122:1594
18. Alkire R, Gracon B (1976) J Electrochem Soc 123:1842
19. Saleh MM, Weidner JW, Ateya BG (1995) J Electrochem Soc 142:4113
20. Cussler LE (1984) Diffusion and mass transfer. Cambridge University Press, Cambridge, p 230
21. Meredith RE, Tobias CW (1962) In: Gerischer H, Tobias CW (eds) Advances in electrochemistry and electrochemical engineering. vol. 2. Wiley, New York, pp 17–48
22. De Vidts P, White RE (1997) J Electrochem Soc 144:1343
23. Newman J (1991) Electrochemical Systems, 2nd ed. Prentice-Hall, Englewood Cliffs, p 552